Supplementary information for

Mixed Oxide Ion−Proton Conductivity and Ionic Migration Mechanism in Isolated Tetrahedral $LaVO_4$ by Acceptor Doping

Xinyue Geng,[a, #] *Gaoqing Hang*,[a, #] *Alberto J. Fernández-Carrión*,[b] *Xing Ming*,[c] *Sihao Deng*,[d] *Lunhua He*,[d, e, f] *Xiaojun Kuang*[a,g] and *Xiaoyan Yang*[a,*]

[a] *MOE Key Laboratory of New Processing Technology for Nonferrous Metal and Materials, Guangxi Key Laboratory of Optical and Electronic Materials and Devices, College of Materials Science and Engineering, Guilin University of Technology, Guilin 541004, P. R. China.*

[b] *Departamento de Química Inorgánica and Instituto de Ciencia de Materiales de Sevilla (ICMS), Centro Mixto CSIC-Universidad de Sevilla, Av. Américo Vespucio, 49, 41092 Sevilla, Spain.*

[c] *College of Science, Guilin University of Technology, Guilin 541004, P. R. China.*

[d] *Spallation Neutron Source Science Center, Dongguan 523803, P. R. China*

[e] *Beijing National Laboratory for Condensed Matter Physics, Institute of Physics, Chinese Academy of Sciences, Beijing 100190, P. R. China*

[f] *Songshan Lake Materials Laboratory, Dongguan 523808, P. R. China*

[g] *College of Chemistry and Bioengineering, Guilin University of Technology, Guilin 541004, P. R. China.*

* E-mail: yangxy@glut.edu.cn

Supplementary Tables and Figures

Table S1. Equations used for the calculation of oxygen vacancy formation in A^{2+} (A = Ca−Ba) doping $LaVO_4$.

Dopant	Equation
Ca^{2+}	$2CaO + O_O^{\times} + 2La_{La}^{\times} \rightarrow 2Ca_{La}^{\cdot\cdot} + V_O^{\cdot\cdot} + La_2O_3$
Sr^{2+}	$2SrO + O_O^{\times} + 2La_{La}^{\times} \rightarrow 2Sr_{La}^{\cdot\cdot} + V_O^{\cdot\cdot} + La_2O_3$
Ba^{2+}	$2BaO + O_O^{\times} + 2La_{La}^{\times} \rightarrow 2Ba_{La}^{\cdot\cdot} + V_O^{\cdot\cdot} + La_2O_3$

Table S2. Buckingham interatomic potential and shell model parameters for A^{2+} (A = Ca−Ba) doping $LaVO_4$ structure.

Interaction	A(eV)	ρ(Å)	C(eV Å)	Y(e)	K(eV $Å^{-2}$)
La^{3+}-O^{2-} [1]	2088.79	0.3460	23.25	-	-
V^{5+}-O^{2-} [2]	668.87	0.4095	0.0	-	-
O^{2-}-O^{2-} [3]	9548.035	0.2192	32.0	-2.04	6.3
Ca^{2+}-O^{2-} [4]	1090.4	0.3437	0.0	3.135	110.2
Sr^{2+}-O^{2-} [2]	1400.0	0.3500	0.0	1.33	21.53
Ba^{2+}-O^{2-} [4]	905.7	0.3976	0.0	9.203	459.2

Table S3. Calculated and experimental structural parameters for monoclinic $LaVO_4$.

Parameters	Calculated	Experimental	$\Delta_{(Calc. - Exp.)}$
a (Å)	7.047	7.981	0.934
b (Å)	7.286	7.270	-0.016
c (Å)	6.725	7.110	-0.385
β (°)	104.850	114.514	9.664
V-O1 (Å)	1.644	1.724	0.079
V-O2 (Å)	1.643	1.720	0.076
V-O3 (Å)	1.578	1.693	0.115
V-O4 (Å)	1.644	1.699	0.055
Mean V-O (Å)	1.627	1.709	0.082
La-O1(×2) (Å)	2.379	2.497	0.118
La-O2(×2) (Å)	2.732	2.568	-0.163
La-O3(×2) (Å)	2.302	2.528	0.226
La-O4(×2) (Å)	2.595	2.533	-0.062
Mean La-O (Å)	2.502	2.532	0.030

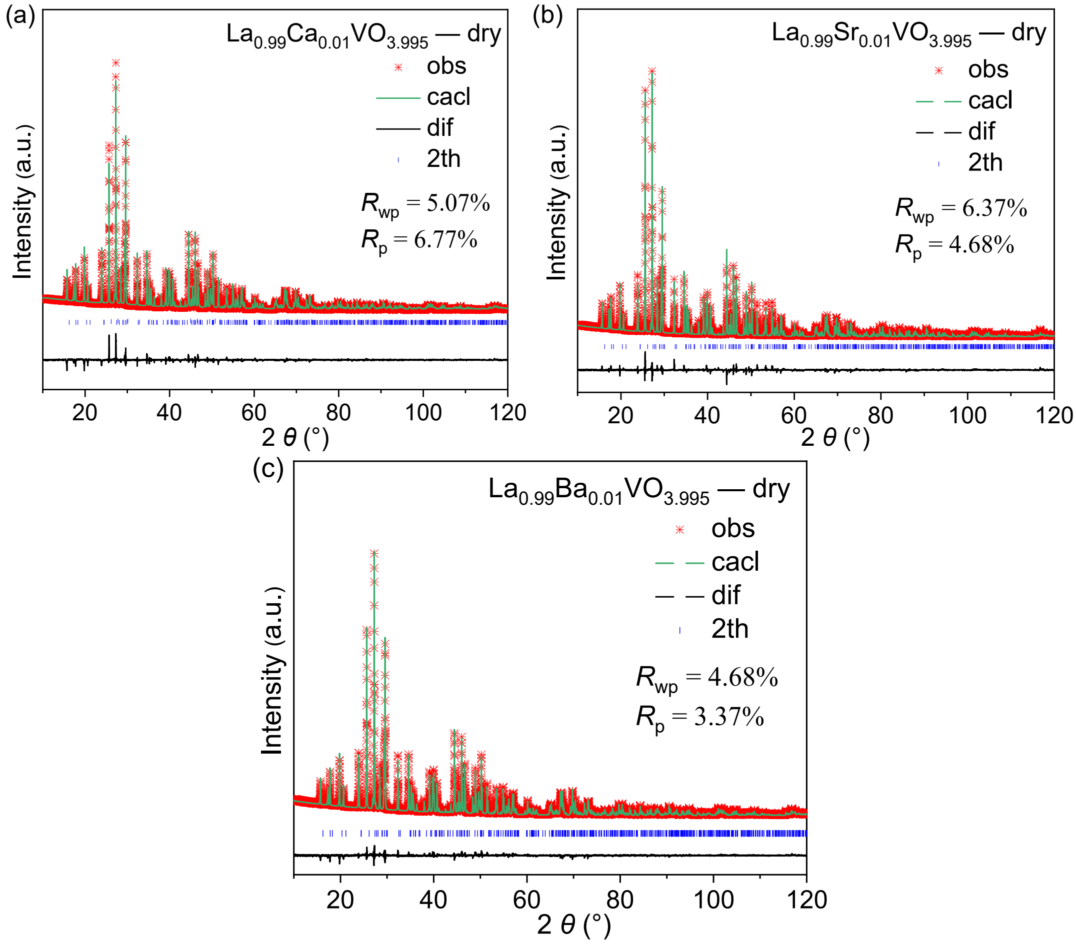

Figure S1. Rietveld plots of XRD pattern of dry (a) $La_{0.99}Ca_{0.01}VO_{3.995}$ (b) $La_{0.99}Sr_{0.01}VO_{3.995}$ and (c) $La_{0.99}Ba_{0.01}VO_{3.995}$, respectively.

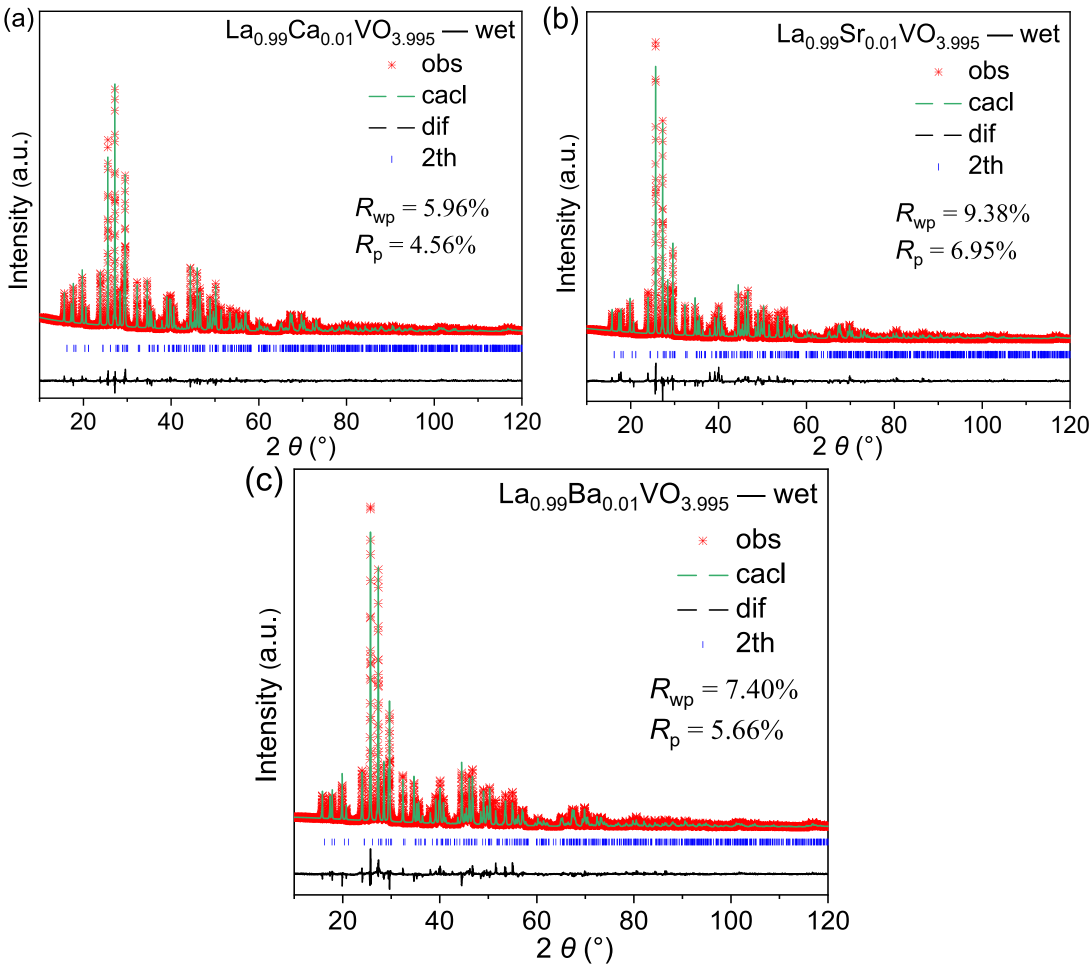

Figure S2. Rietveld plots of XRD pattern of wet (a) $La_{0.99}Ca_{0.01}VO_{3.995}$ (b) $La_{0.99}Sr_{0.01}VO_{3.995}$ and (c) $La_{0.99}Ba_{0.01}VO_{3.995}$, respectively.

Table S4. Refined cell parameters of $La_{0.99}A_{0.01}VO_{3.995}$(A = Ca– Ba) and $LaVO_4$*.

Composition	Environ-ment	*a* (Å)	*b* (Å)	*c* (Å)	*β* (°)	*V* (Å^3)
$La_{0.99}Ca_{0.01}VO_{3.995}$	dry air	7.03888(5)	7.27603(5)	6.72019(5)	104.8859(4)	332.625(5)
$La_{0.99}Sr_{0.01}VO_{3.995}$	dry air	7.04744(3)	7.28593(3)	6.72758(3)	104.8805(2)	333.858(3)
$La_{0.99}Ba_{0.01}VO_{3.995}$	dry air	7.04764(2)	7.28637(3)	6.72674(2)	104.8685(3)	333.864(2)
$La_{0.99}Ca_{0.01}VO_{3.995}$	wet air	7.04672(8)	7.28514(8)	6.72692(7)	104.8823(4)	333.752(7)
$La_{0.99}Sr_{0.01}VO_{3.995}$	wet air	7.0475(1)	7.2868(1)	6.7275(1)	104.8787(7)	333.90(1)
$La_{0.99}Ba_{0.01}VO_{3.995}$	wet air	7.0491(1)	7.2874(1)	6.7281(1)	104.8731(1)	334.04(1)

*The lattice parameter of $LaVO_4$: space group $P2_1/n$, $Z = 4$, $a = 7.04653(3)$ Å, $b = 7.28419(3)$ Å, $c = 6.72492(3)$ Å, $\beta = 104.8636(2)$, $V = 333.629(3)$ Å^3.

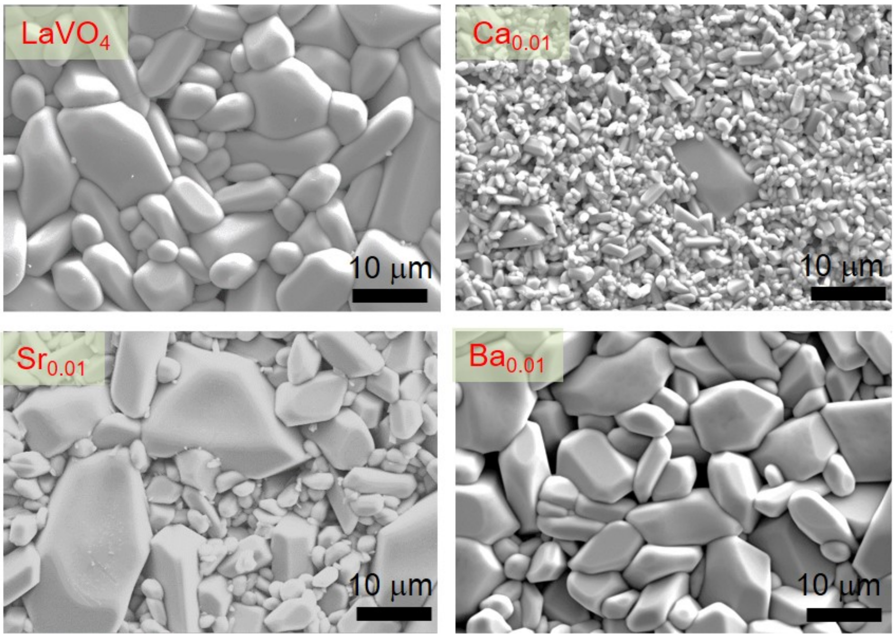

Figure S3. The surface morphology of $LaVO_4$ and $La_{0.99}A_{0.01}VO_{3.995}$ (A = Ca, Sr and Ba) ceramic pellets.

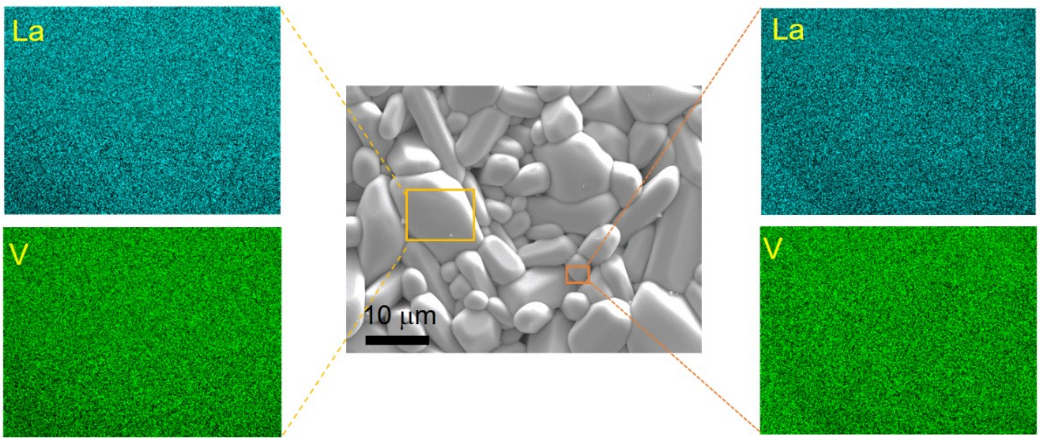

Figure S4. Selected SEM-EDS elemental mapping of $LaVO_4$ ceramic pellet. The ratios of La/V is 1.01(3) : 1.00(3).

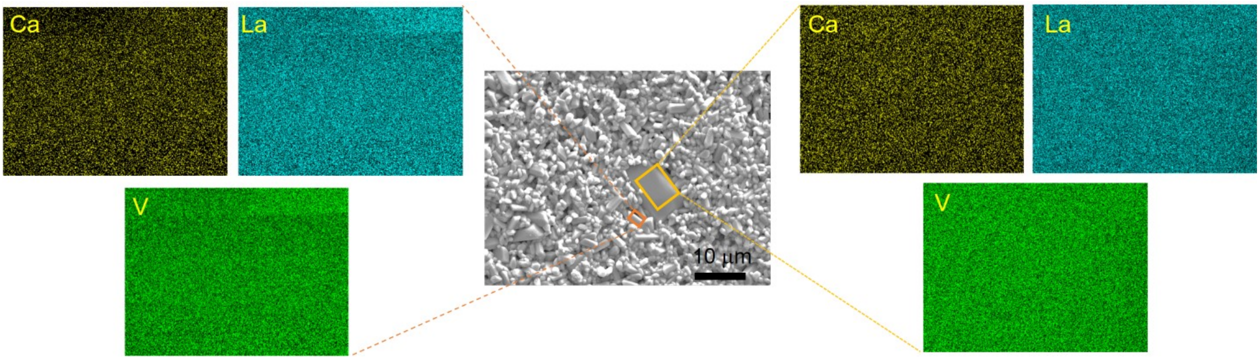

Figure S5. Selected SEM-EDS elemental mapping for $La_{0.99}Ca_{0.01}VO_{3.995}$ ceramic pellet. The ratios of La/Ca are 0.99(3) : 0.01(3) and 0.99(1) : 0.01(1) for the small and big grain, respectively.

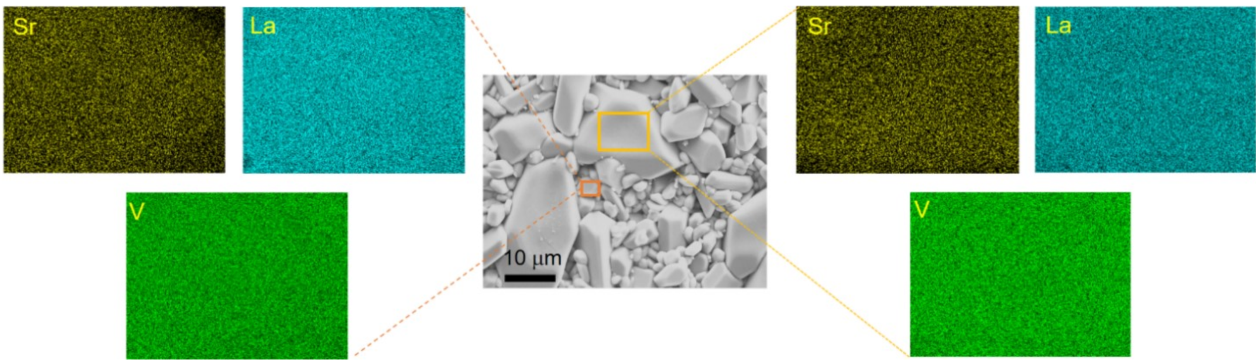

Figure S6. Selected SEM-EDS elemental mapping for $La_{0.99}Sr_{0.01}VO_{3.995}$ ceramic pellet. The ratios of La/Sr are 0.99(5) : 0.01(5) and 0.99(1) : 0.01(1) for the small and big grain, respectively.

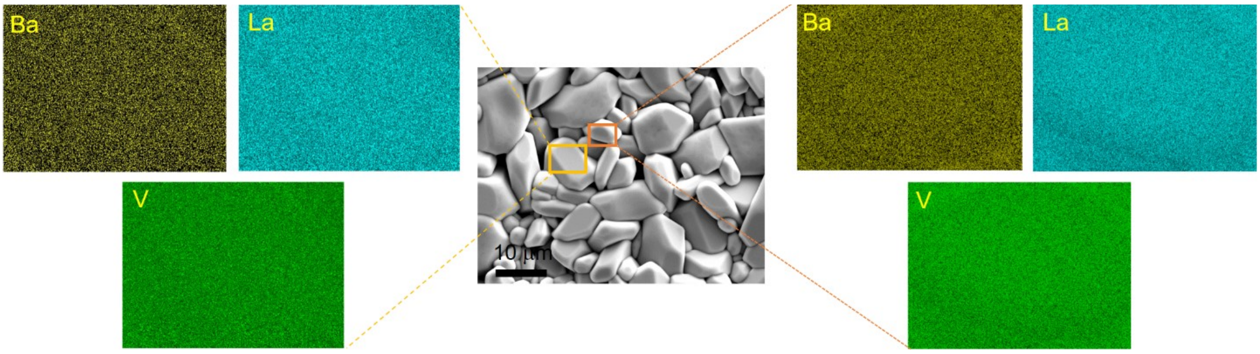

Figure S7. Selected SEM-EDS elemental mapping for $La_{0.99}Ba_{0.01}VO_{3.995}$ ceramic pellet. The ratios of La/Ba are 0.99(2) : 0.01(2) and 0.99(6) : 0.01(6) for the small and big grain, respectively.

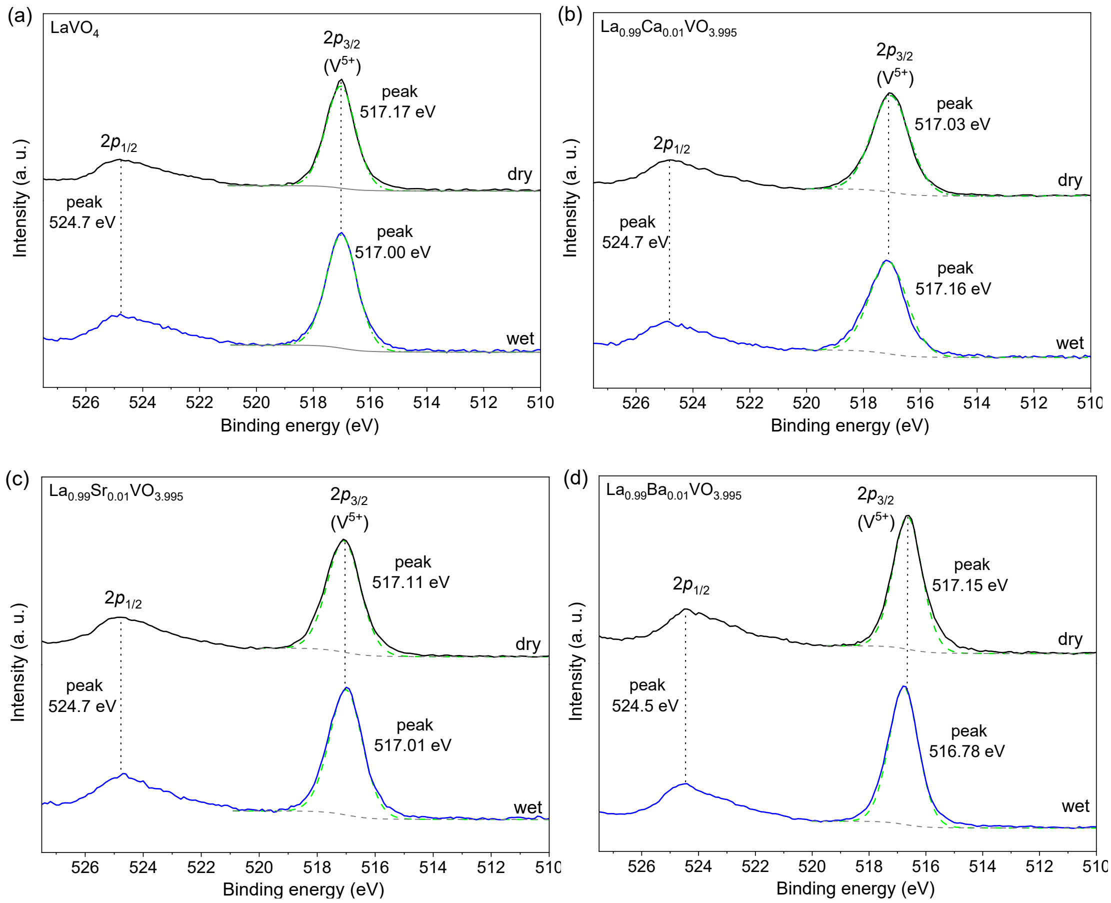

Figure S8. V 2*p* peaks XPS spectra of (a) $LaVO_4$ (b) $La_{0.99}Ca_{0.01}VO_{3.995}$ (c) $La_{0.99}Sr_{0.01}VO_{3.995}$ (d) $La_{0.99}Ba_{0.01}VO_{3.995}$ powders.

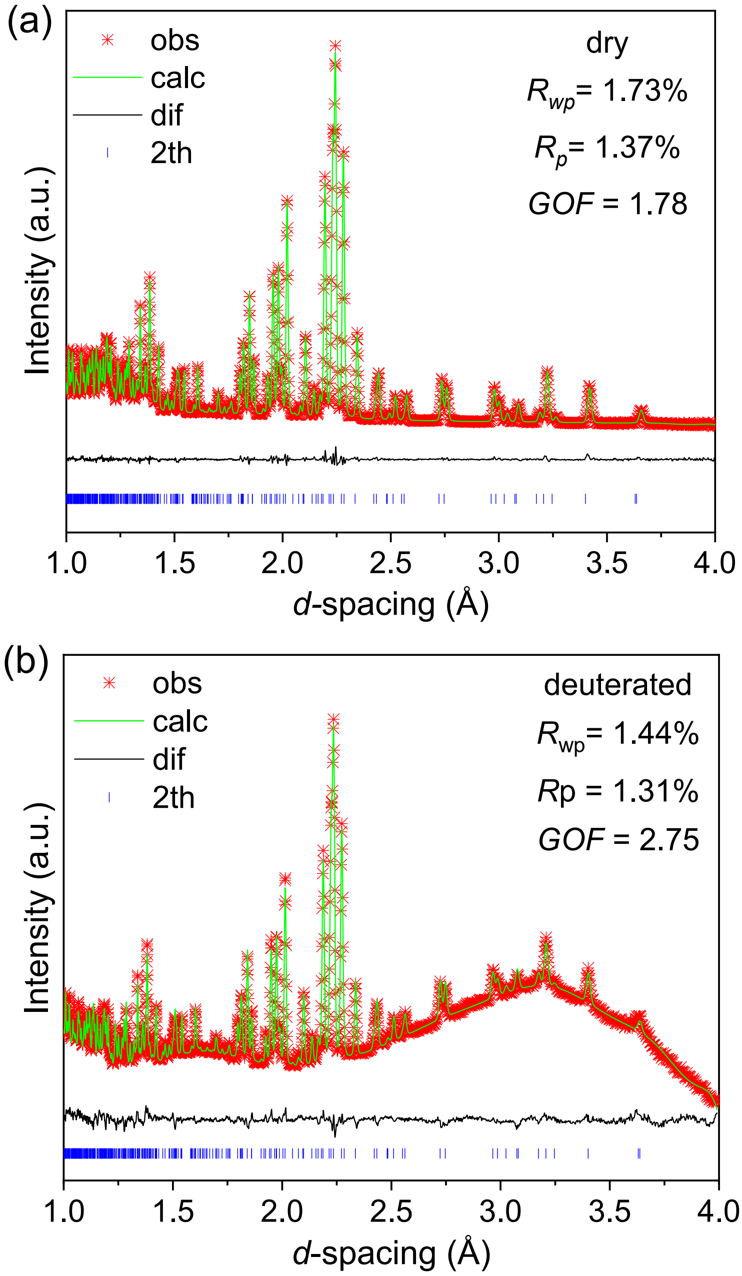

Figure S9. Rietveld refinement plots of NPD pattern for dry and deuterated $La_{0.99}Sr_{0.01}VO_{3.995}$ powders.

Table S5. (a) Fractional atomic coordinates and isotropic atomic displacement parameters (in Å^2) and (b) Anisotropic displacement parameters of oxygen atoms for dry $La_{0.99}Sr_{0.01}VO_{3.995}$*.

(a)	Site	*x*	*y*	*z*	occupancy	U_{eq} (Å^2) [a]
La/Sr	4*e*	0.2759(6)	0.1569(1)	0.1030(1)	0.99(La)/0.01(Sr)	1.65(1)
V	4*e*	0.3011(1)	0.1655(2)	0.6199(2)	1	1.32(3)[a]
O1	4*e*	0.2442(1)	-0.0013(1)	0.4276(2)	1	-
O2	4*e*	0.3871(1)	0.3431(1)	0.4969(1)	1	-
O3	4*e*	0.4821(1)	0.1063(1)	0.8230(1)	1	-
O4	4*e*	0.1186(2)	0.2202(1)	0.7263(2)	1	-

(b)	U_{11}(Å^2)	U_{22}(Å^2)	U_{33}(Å^2)	U_{12}(Å^2)	U_{13}(Å^2)	U_{23}(Å^2)
O1	0.0287(8)	0.0218(7)	0.0169(7)	0.003(1)	0.005(1)	0.002(1)
O2	0.0235(6)	0.0199(6)	0.0259(7)	0.004(1)	0.007(1)	0.005(1)
O3	0.0285(8)	0.0230(8)	0.0207(8)	0.005(1)	0.003(1)	0.001(1)
O4	0.0017(6)	0.0219(8)	0.0228(8)	0.000(1)	0.004(1)	0.003(1)

*Space group: $P2_1/n$; a = 7.0367(1) Å, b = 7.27413(4) Å, c = 6.7181(1) Å, $\alpha = \gamma$ = 90°, β = 104.8750(7) °, V =332.353(3) Å^3.

[a] The atomic coordinates and isotropic structural parameters of V are obtained from XRD Rietveld refinement because of the low sensitivity of neutrons to vanadium.

Table S6. (a) Fractional atomic coordinates and isotropic atomic displacement parameters (in Å^2) and (b) Anisotropic displacement parameters of oxygen atoms for hydrated $La_{0.99}Sr_{0.01}VO_{3.995}$*.

(a)	Site	*x*	*y*	*z*	occupancy	U_{eq} (Å^2) [a]
La/Sr	4*e*	0.2754(4)	0.1571(4)	0.1035(3)	0.99(La)/0.01(Sr)	1.44(3)
V	4*e*	0.3011(1)	0.1655(2)	0.6199(2)	1	1.32(3)
O1	4*e*	0.2413(5)	-0.0023(5)	0.4272(6)	1	-
O2	4*e*	0.3864(5)	0.3418(5)	0.4961(5)	1	-
O3	4*e*	0.4821(5)	0.1051(4)	0.8214(5)	1	-
O4	4*e*	0.1198(6)	0.2179(5)	0.7285(6)	1	-

(b)	U_{11}(Å^2)	U_{22}(Å^2)	U_{33}(Å^2)	U_{12}(Å^2)	U_{13}(Å^2)	U_{23}(Å^2)
O1	0.005(3)	-0.001(3)	-0.002(2)	0.002(5)	0.013(5)	0.010(5)
O2	0.001(3)	0.003(3)	-0.002(3)	0.002(6)	0.010(5)	0.001(5)
O3	-0.003(4)	-0.000(3)	-0.001(3)	0.006(5)	-0.003(5)	0.008(4)
O4	0.021(3)	-0.007(3)	0.004(3)	0.001(5)	0.011(5)	0.004(4)

*Space group: *P2₁/n*; a = 7.0380(5) Å, b= 7.2748(1) Å c = 6.7176(5) Å, $\alpha = \gamma = 90°$, β = 104.881(1) °, V = 332.409(8) Å^3.

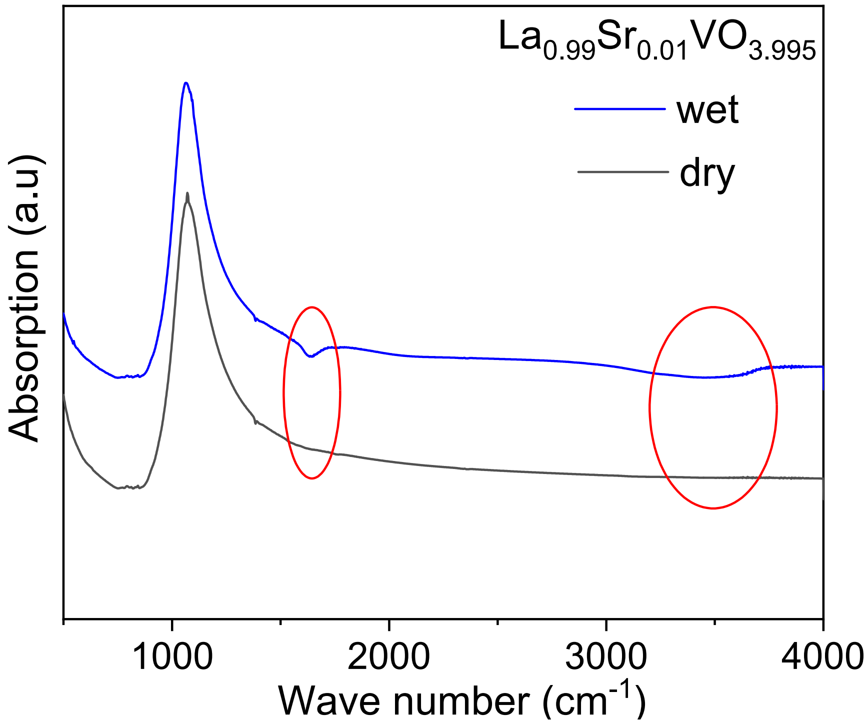

Figure S10. Infrared absorption spectrum of dry and wet $La_{0.99}Sr_{0.01}VO_{3.995}$ powders.

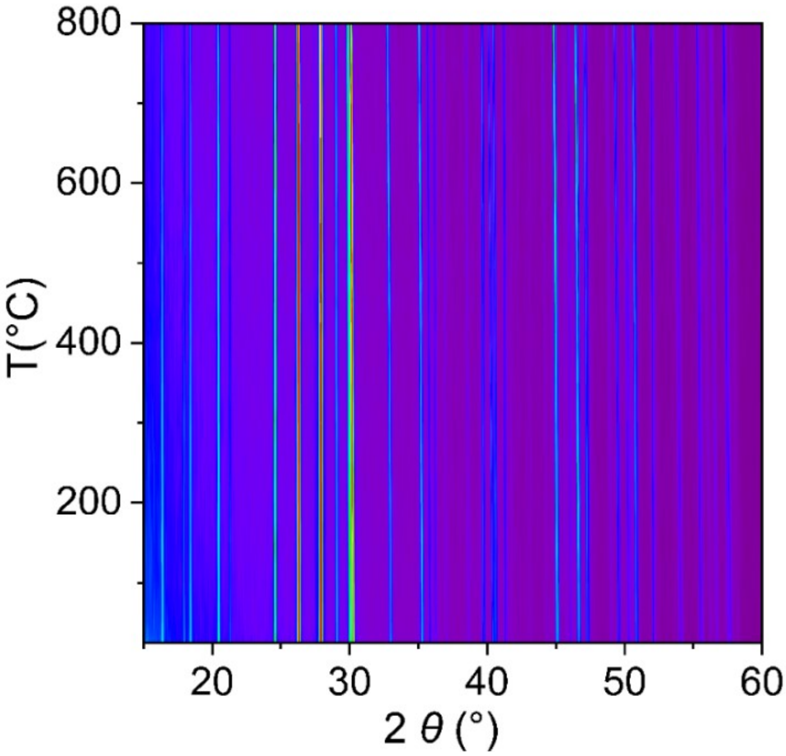

Figure S11. "Film plot" of in situ VT-XRD data for $LaVO_4$ on heating.

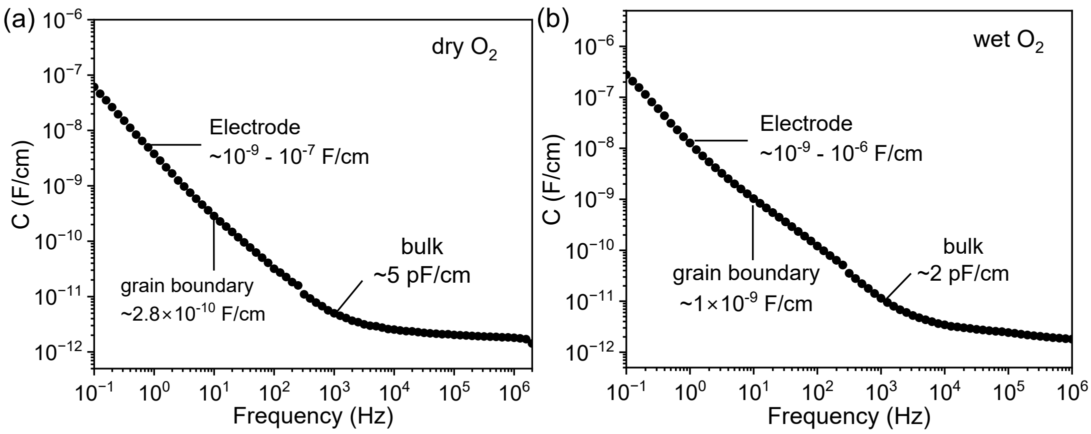

Figure S12. The frequency dependency of capacitance for $La_{0.99}Sr_{0.01}VO_{3.995}$ ceramic at 350°C under (a) dry O_2 (b) wet O_2.

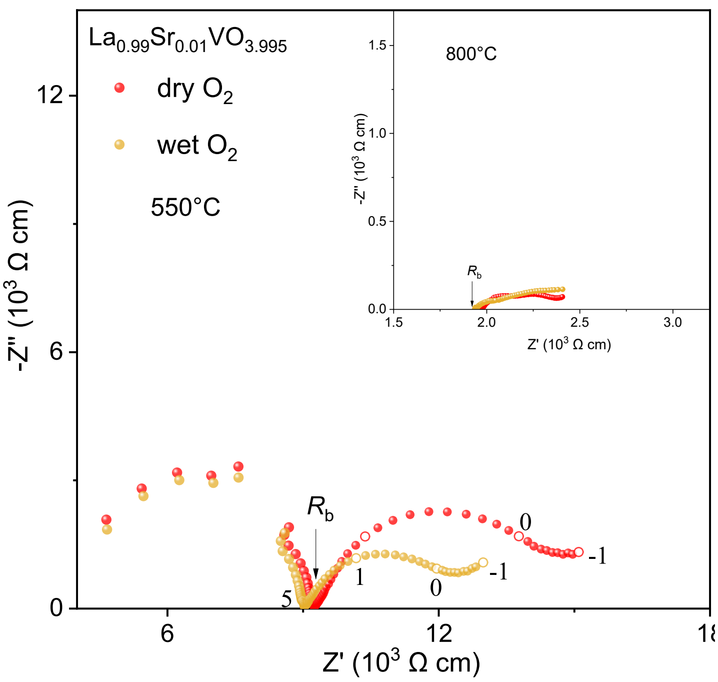

Figure S13. Complex impedance plots of $La_{0.99}Sr_{0.01}VO_{3.995}$ pellet at 550°C and 800°C (inset) under dry and wet O_2 atmosphere. R_b denotes bulk resistivity. The numbers indicate the logarithm values of the selected frequencies marked by hollow circles.

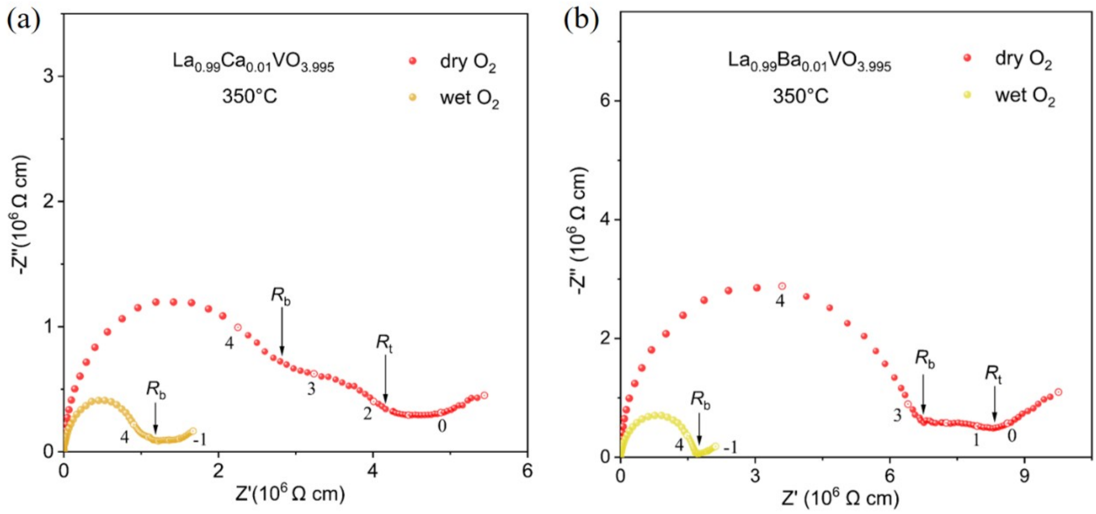

Figure S14. Complex impedance plots of (a) $La_{0.99}Ca_{0.01}VO_{3.995}$ and (b)$La_{0.99}Ba_{0.01}VO_{3.995}$ pellet recorded at 350°C under dry and wet O_2. R_b and R_t denote bulk and total resistivity, respectively. The numbers indicate the logarithm values of the selected frequencies marked by hollow circles.

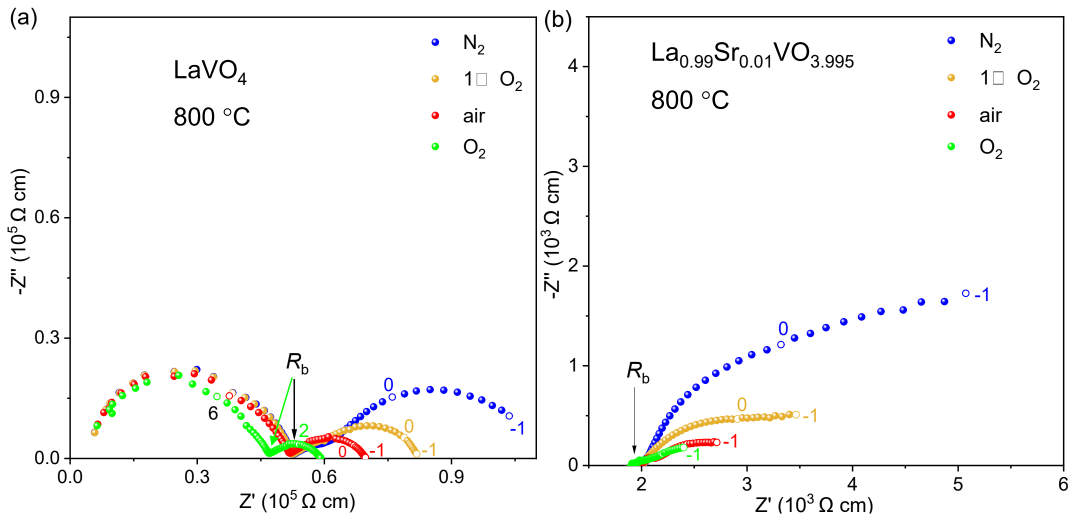

Figure S15. Complex impedance plots of $LaVO_4$ and $La_{0.99}Sr_{0.01}VO_{3.995}$ ceramics at 800°C under N_2, 1% O_2, air and O_2.

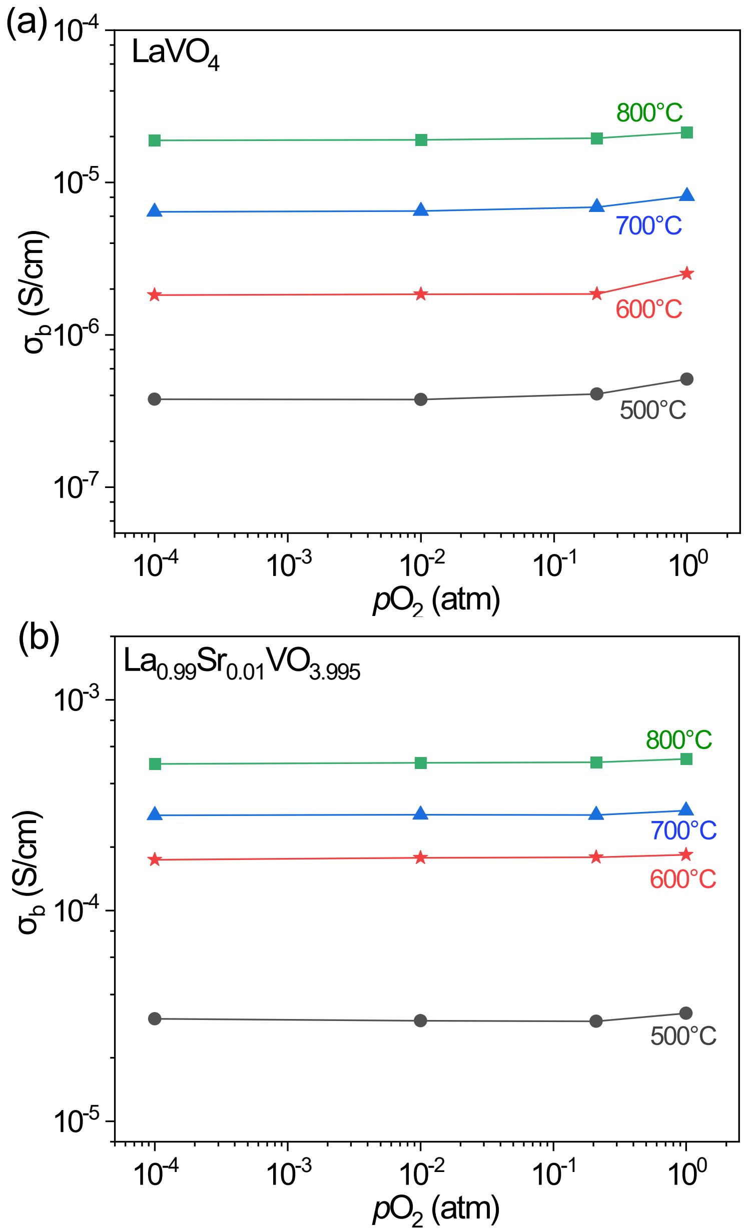

Figure S16. The pO_2 dependency of the bulk conductivities for (a) $LaVO_4$ (b) $La_{0.99}Sr_{0.01}VO_{3.995}$ within 500°C−800°C.

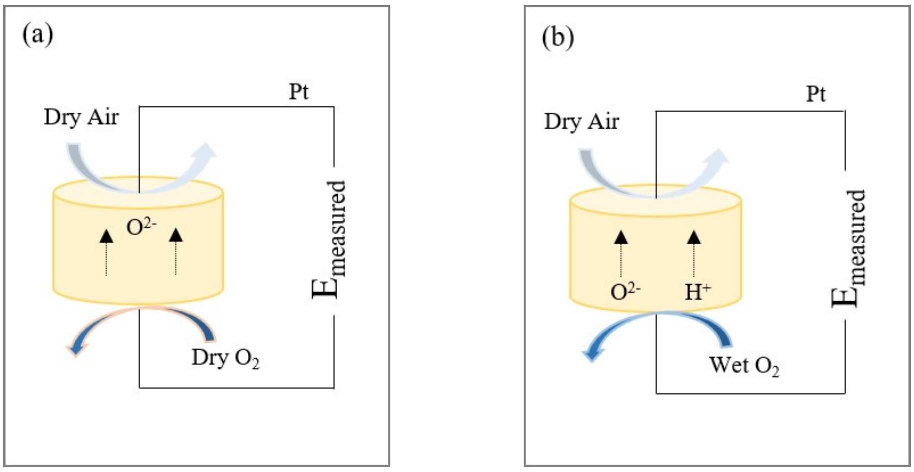

Figure S17. Diagram for Electromotive Force measurement in (a) $dry\ O_2||Air$ and (b) $wet\ O_2||Air$ condition.

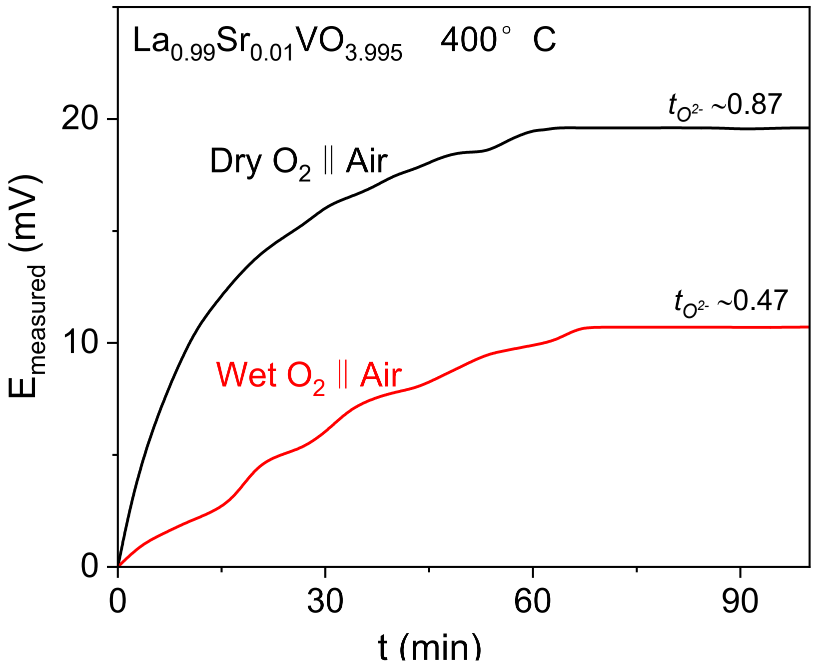

Figure 18. The measured electromotive force ($E_{measured}$) of $La_{0.99}Sr_{0.01}VO_{3.995}$ ceramic pellet under $dry\ O_2||Air$ and $wet\ O_2||Air$ condition.

Table S7. Lattice parameter and free energy of A^{2+} doping $LaVO_4$ structure.

	H	Distance of O-H(Å)		Distance of O-A(Å)		Distance of H-A(Å)		Free energy(eV)
		initial	final	initial	final	initial	final	
Sr	H1-1	1.11	1.04	2.48	2.66	2.66	2.56	0*
	H3-1	1.11	1.05	2.47	2.65	2.70	2.53	0.01
	H3-2	1.11	1.02	5.10	5.14	6.94	5.91	0.69
	H3-3	1.11	1.01	4.52	4.85	5.36	5.69	0.68
	H3-4	1.11	1.09	4.52	4.56	5.55	5.34	0.62
	H2	1.11	1.02	2.50	2.65	2.25	2.45	0.35
	H4	1.11	1.03	2.53	2.70	2.28	2.46	0.70
	H5	1.11	1.01	2.51	2.60	2.65	2.79	0.64
	H6	1.11	1.09	2.64	2.89	1.53	2.45	0.65
Ba	H1-1	1.11	1.05	2.47	2.75	2.70	2.62	0.32
	H3-1	1.11	0.77	2.48	2.53	2.66	2.66	0.26
Ca	H1-1	1.11	0.96	2.47	2.48	2.70	2.64	0.03
	H3-1	1.11	0.99	2.48	2.46	2.66	2.65	0.02

* The actual energy value is -1649.790205eV.

Reference

1. L. Minervini, R. W. Grimes and K. E. Sickafus, Disorder in pyrochlore oxides, *J. Am. Ceram. Soc.*, 2000, **83**, 1873−1878.
2. X. Yang, X. Zeng, X. Ming, L. Yang, A. J. Fernández-Carrión, S. Deng, L. He and X. Kuang, Oxide-ion conductivity optimization in $BiVO_4$ scheelite by an acceptor doping strategy, *Inorg. Chem. Front.*, 2022, **9**, 2644−2658.
3. L. Minervini, M. O. Zacate and R. W. Grimes, Defect cluster formation in M_2O_3-doped CeO_2, *Solid State Ionics*, 1999, **116**, 339−349.
4. A. N. Cormack, C. R. A. Catlow, G. V. Lewis and C. M. Freeman, Defect behaviour in oxides, *MRS Online Proceedings Library*, 1985, **63**, 55−60.